Chapter 4

Phase-Controlled Apertures

When a number of slave SCLs are locked to the same master laser, they all inherit the same coherence properties, as shown in chapter 3. Further, the heterodyne OPLL configuration allows the optical phase to be controlled by varying the electronic phase of the RF offset signal, enabling phase-controlled apertures. In this chapter, we explore applications of such phase-controlled apertures in coherent power-combining and electronic beam-steering.

4.1 Coherent Power-Combining

High power lasers with ideal (diffraction-limited) beam quality are sought after in a multitude of applications including scientific research, materials processing and industrial applications, and research in this direction has been in progress ever since the invention of the laser. While high power (few kilowatts single mode) fiber laser systems have been demonstrated [96, 97], their output powers will ultimately be limited by nonlinear effects in the fiber and material damage. An alternate approach to obtain high power laser radiation with excellent beam quality is by combining a large number of laser emitters with lower power outputs [98–100]. In particular, coherent beam-combining (CBC) is a very promising approach to synthesize high-power optical sources with ideal beam quality. Various coherent beam-combining schemes have been demonstrated by different groups, including evanescent wave-coupling, self-organizing [99], injection locking [100], common resonator [101] and

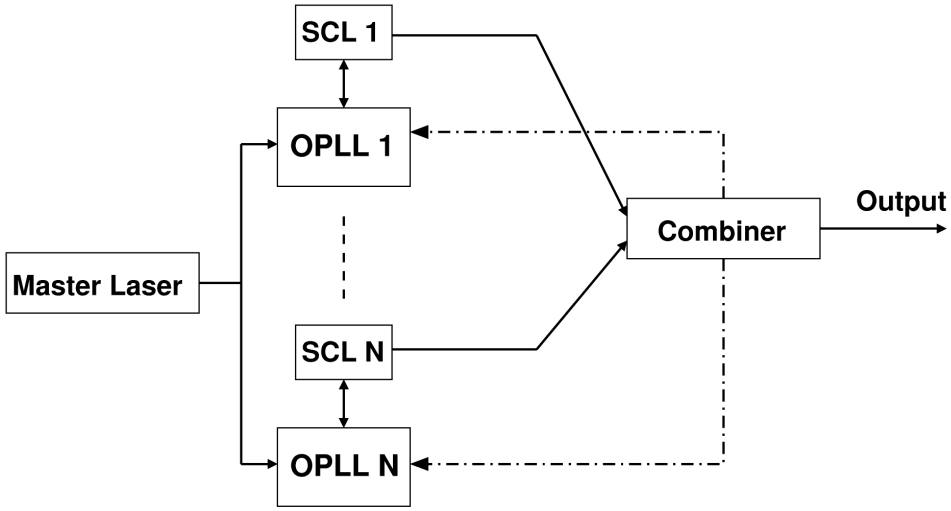

Figure 4.1. Coherent power-combining scheme using heterodyne SCL-OPLLs. Individual SCLs all lock to a common master laser, thus forming a coherent array. The outputs of the individual lasers are coherently combined to obtain a high power single-mode optical beam.

active feedback [102] approaches. While it is desirable to match the relative amplitudes, phases, polarizations and pointing directions of all the component beams to achieve maximum efficiency in a CBC scheme [98], the precise control over the optical phase offers the biggest challenge. Various active feedback approaches for phase control have been demonstrated, where the phase error between the combining beams is fed back to a servo system that includes phase actuators, which could be optical phase modulators [100], acousto-optic modulators [102] or fiber stretchers [103].

In this section, we describe an alternative active feedback approach for CBC where the outputs of an array of SCLs phase-locked to a common master laser are coherently combined to obtain a single high power coherent optical beam as shown in figure 4.1. The use of SCLs has many distinct advantages such as their compactness, high efficiency, low cost and high output power, thereby making them attractive candidates for coherent power combination. The small size and high output powers of SCLs offer the potential for the combination of a number of SCLs on a single chip, leading to extremely compact high power sources. The optical phase of each SCL in a coherent combining scheme can then be controlled *electronically*, which eliminates the need for optical phase or frequency shifters that are bulky, expensive and require the use of

large voltages.

Coherent power combination results in optical beams with superior beam quality and larger peak intensities as compared to incoherent power addition. There are two approaches to CBC [98]: (a) the filled-aperture approach where multiple beams are combined into a single beam using a beam-combiner, and (b) the tiled-aperture approach, where the outputs of the individual emitters are adjacent to each other. One of the key aspects in either approach is the control over the relative phases of the individual emitters at the beam combiner. In this section, we concentrate on the filled-aperture approach, while tiled-aperture beam-combining and wavefront control is described in section 4.2.

4.1.1 Experiment

A schematic of the filled-aperture power-combining experiment is shown in figure 4.2(a). Two slave SCLs are locked to a common master laser using fiber-based heterodyne OPLLs as shown in figure 2.1. A common RF offset signal (in the range of $\sim$0.8–1.7 GHz) is fed to each loop. It is only necessary to use a small fraction of the SCL output in the feedback loop, and the remaining power is used for power combination. The outputs of the two SCLs are combined using a 2×1 fiber combiner, and the output is measured on an oscilloscope. The result of the experiment with high power MOPAs as slave SCLs (QPC Lasers, see table 2.1) is shown in figure 4.2(b). For time $<$2.5 seconds, one of the lasers is unlocked, and the resultant incoherent addition results in high frequency oscillations on the oscilloscope at the (time-varying) beat frequency between the two SCLs.

When both the loops are in lock (time $>$2.5 seconds), the result is a "DC" signal that varies very slowly (on the timescale of a few seconds). The combined power is given by

$$P_c = P_0(1 + \cos\theta), \tag{4.1}$$

where θ is the phase difference between the two combining beams. For maximal power-combining efficiency, we need $\theta = 0$. There are two causes of a deviation from

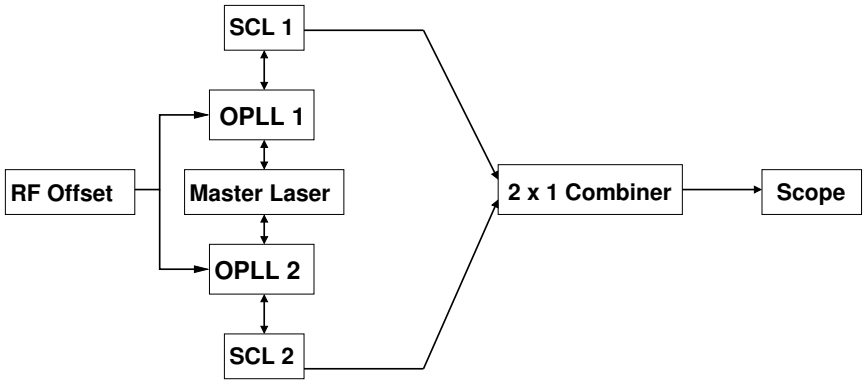

(a)

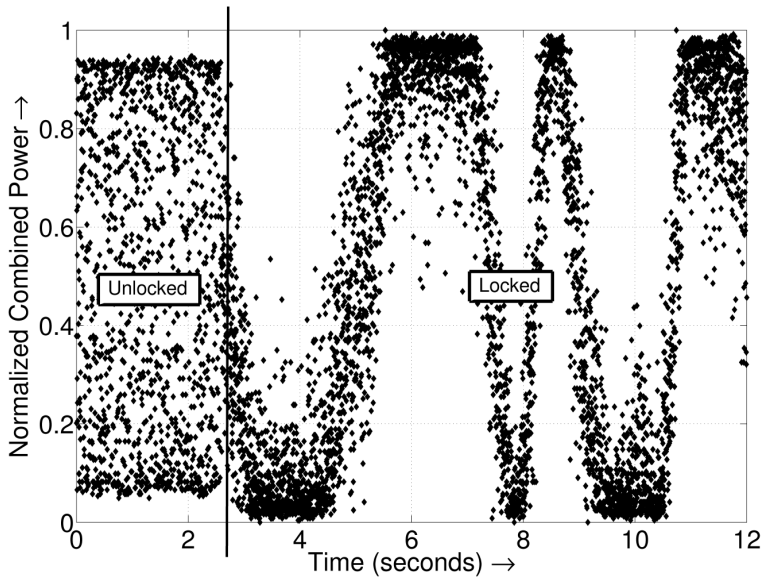

(b)

Figure 4.2. (a) Coherent combination schematic. Two SCLs are locked to a common master laser at a common offset, and the combined output is measured on an oscilloscope. (b) Experimentally measured combined power using two high power MOPAs as slave lasers phase-locked to a common master laser. For $t < 2.5$ seconds, one of the OPLLs is not in lock, and the result is the incoherent power addition of the two lasers.

this ideal value. In fiber-based systems, variations in the differential optical paths of the two combining beams cause a change in phase; this is the cause of the slow drift. The differential phase change may be several full waves, especially if fiber amplifiers are used at the SCL outputs, and a technique to eliminate the effect of this slow drift is described in the next section. In addition to the slow drift, the combined power signal also shows fast variations due to the residual phase noise between the two combined beams. The RMS value of the residual phase error is estimated from the *fast* variations in the measurement in figure 4.2(b) to be about 0.39 radians. This corresponds to a residual phase error of $0.39/\sqrt{2} = 0.28$ radians in each OPLL, which is in excellent agreement with the measured value in table 2.1.

4.1.2 Phase Control Using a VCO

We now describe a novel electronic feedback scheme developed to correct for the slow drift in the relative phase between the optical beams. The variations in the differential optical paths traversed by combining beams is traditionally controlled using a piezoelectric fiber stretcher, an acousto-optic modulator or an optical phase modulator [100, 102, 103]. The phase of the phase-locked SCL in a heterodyne OPLL follows the phase of the RF offset signal, and this allows for the electronic control over the optical phase. The phase of the RF offset signal can be tuned using an RF phase shifter, but this method has the same shortcomings as an optical phase shifter, i.e., insufficient dynamic range to correct for large phase errors [66]. Typical optical or RF phase modulators have a dynamic range of 2π radians, and complicated reset-circuitry is often necessary to increase the dynamic range. In the alternative phase-control scheme described here, the correction signal is provided by an electronic VCO. In addition to acting as an integrating phase shifter with practically infinite dynamic range, the VCO also provides the RF offset signal to the heterodyne OPLL.

A schematic of the power-combining experiment with the VCO correction loop is shown in figure 4.3(a). Two SCLs are phase-locked to a common master laser using heterodyne OPLLs. While an RF source provides a fixed offset signal to one OPLL,

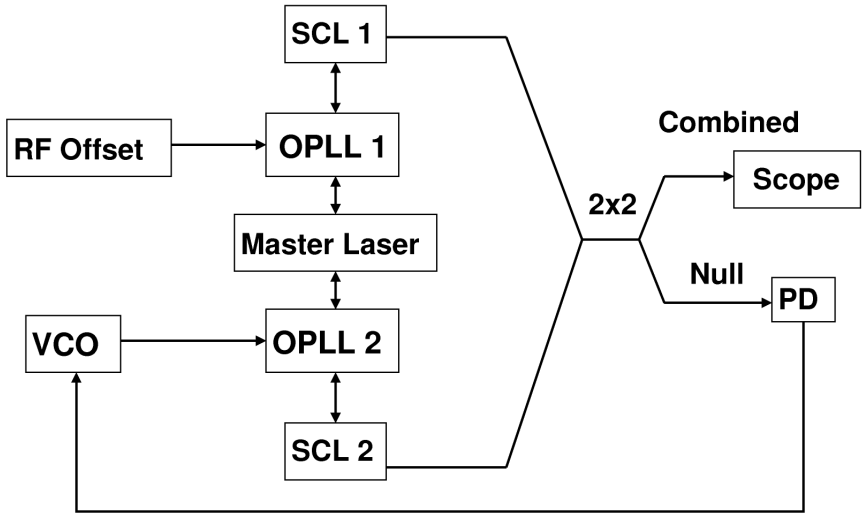

(a)

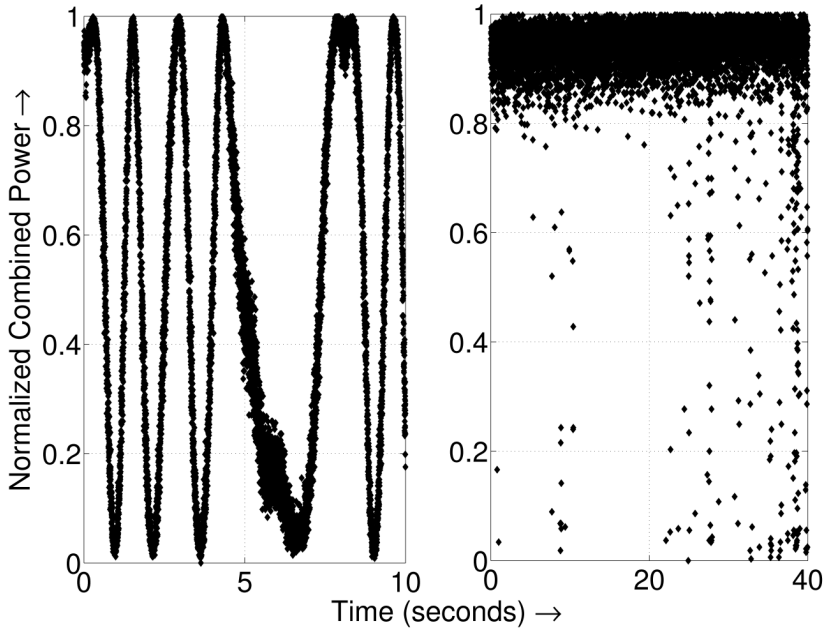

(b)

Figure 4.3. (a) Schematic of the coherent combination experiment with additional electronic phase control. A VCO provides the offset signal to the second OPLL, and also acts as an integrating phase shifter to correct for variations in the differential optical path length. (b) Experimentally measured combined power using external cavity SCLs at 1064 nm, without (left) and with (right) the VCO loop connected. The power-combining efficiency with the VCO loop is 94%.

the offset signal to the other OPLL is provided by a VCO. The nominal free-running frequency of the VCO is chosen to be equal to the frequency of the RF source. The outputs of the two lasers are combined using a 2×2 fiber coupler. One of the outputs of the coupler (the "combined" output) is observed on an oscilloscope, while the other output (the "null" output) is amplified and fed into the control port of the VCO. The measured combined power signal, with and without the VCO control loop, in the power-combining experiment using external cavity lasers (Innovative Photonic Solutions, see table 2.1) is shown in figure 4.3(b). A stable power-combining efficiency of 94% is obtained using the VCO phase-correction loop. This efficiency is mainly limited by the jitter of the free-running frequency of the VCO used in the experiment and not by the residual phase noise in the OPLL, and can therefore be further improved by the use of cleaner VCOs. The VCO frequency jitter is also responsible for the occasional cycle slips seen in figure 4.3(b).

4.1.2.1 Steady-State Analysis

We begin by noting that the behavior of SCL 1 in the system shown in figure 4.3(a) is well understood, both in terms of its steady state and transient performance. Therefore, we will confine ourselves to the analysis of the OPLL with SCL2, and the effects of the power combination feedback on this loop. We first find the steady state operating point of this part of the system. Under steady state, the system can be modeled as in figure 4.4, where the intrinsic phase noise of the lasers, thermal and mechanical fluctuations in the fiber, and the phase noise of the VCO are neglected. The $1-\cos(.)$ term reflects the fact that the output of this detector is out of phase with the combined output in equation (4.1). We assume that the loop filters $G_2(s)$ and $G_v(s)$ have unity gain at DC. We can then write down the equations for the phase "error" signals θ_2 and θ_v at the outputs of the photodetectors:

$$\omega_m t - \left(\omega_{s2}^{fr} t + \int K_2 \sin\theta_2 \, dt\right) + \omega_v^{fr} t + \phi_v = \theta_2, \tag{4.2}$$

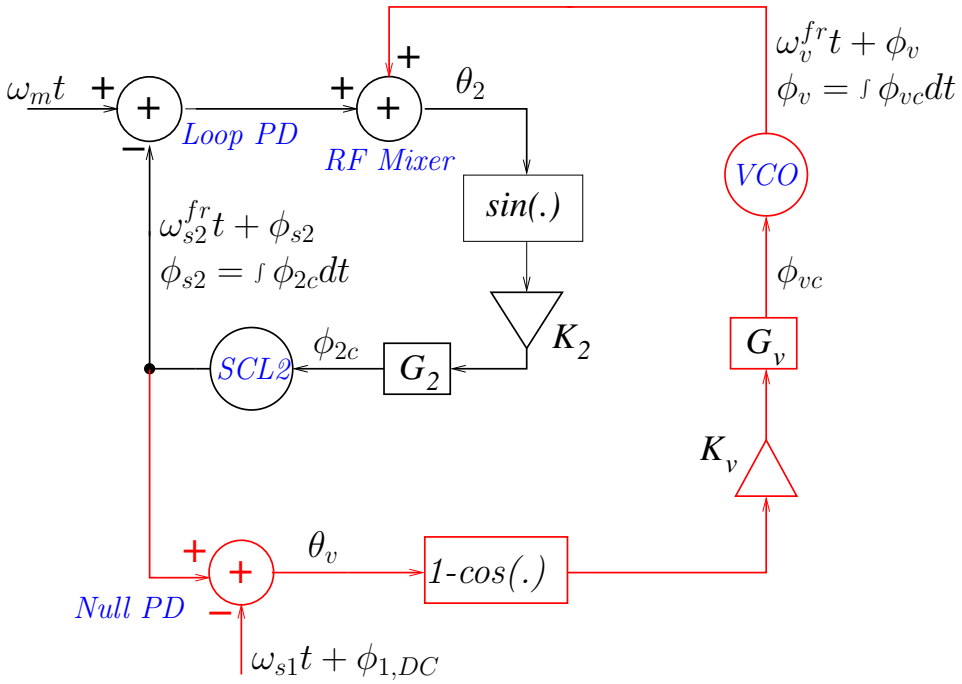

Figure 4.4. Steady-state model for the loop OPLL 2 shown in figure 4.3(a). The frequency of SCL 1 *in its locked state* is denoted by ω_{s1}, and $\phi_{1,DC}$ represents any constant phase difference between the lasers at the "null" photodetector input. The free-running frequencies of Laser 1 and the VCO are ω_{s2}^{fr} and ω_v^{fr} respectively. The frequency of the master laser is ω_m.

so that

$$\dot{\theta_2} = \left(\omega_m - \omega_{s2}^{fr} + \omega_v^{fr}\right) - K_2 \sin\theta_2 + \dot{\phi_v}. \tag{4.3}$$

Similarly, at the other photodetector,

$$\omega_{s2}^{fr} t + \int K_2 \sin\theta_2 \, dt - \omega_{s1} t - \phi_{1,DC} = \theta_v, \tag{4.4}$$

$$\dot{\theta_v} = \left(\omega_{s2}^{fr} - \omega_{s1}\right) + K_2 \sin\theta_2, \tag{4.5}$$

since $d\phi_{1,DC}/dt = 0$. The VCO phase ϕ_v is given by

$$\phi_v = \int K_v \left(1 - \cos\theta_v\right) \, dt, \tag{4.6}$$

$$\dot{\phi_v} = K_v \left(1 - \cos\theta_v\right). \tag{4.7}$$

The steady state phase errors θ_2 and θ_v are found by setting their time derivatives to zero in equations (4.3) and (4.5), and using the value of $\dot{\phi_v}$ obtained in equation (4.7):

$$\begin{aligned} \theta_{2,s} &= \sin^{-1} \frac{\left(\omega_{s1} - \omega_{s2}^{fr}\right)}{K_2}, \\ \theta_{v,s} &= \cos^{-1} \left(1 - \frac{\left(\omega_{s1} - \omega_m - \omega_v^{fr}\right)}{K_v}\right). \end{aligned} \tag{4.8}$$

Now, we note that ω_{s1} represents the frequency of SCL 1 *when it is locked* to the master laser at a frequency offset of ω_{RF}, so that

$$\omega_{s1} = \omega_m + \omega_{RF}. \tag{4.9}$$

When this is plugged back into equations (4.8), we find the steady state phase errors:

$$\begin{aligned}\theta_{2,s} &= \sin^{-1}\frac{\left(\omega_m + \omega_{RF} - \omega_{s2}^{fr}\right)}{K_2},\\ \theta_{v,s} &= \cos^{-1}\left(1 - \frac{\left(\omega_{RF} - \omega_v^{fr}\right)}{K_v}\right).\end{aligned} \tag{4.10}$$

Plugging this back into the model in figure 4.4, we find the frequencies of SCL2 and the VCO in lock:

$$\begin{aligned}\omega_{s2} &= \omega_m + \omega_{RF},\\ \omega_v &= \omega_{RF}.\end{aligned} \tag{4.11}$$

The above results are consistent with the intuitive interpretation that SCL2 is locked to the master laser at the offset frequency ω_v, and ω_v in turn is locked to the frequency reference ω_{RF}.

The steady-state error $\theta_{v,s}$ in equation (4.10) represents the phase difference between the two combining SCLs in equation (4.1), and it is clear that a large K_v is desirable so that $\theta_{v,s}$ is close to zero,[1] and a high efficiency is achieved. Further, $\theta_{v,s}$ can be tuned by varying the free-running VCO frequency ω_v^{fr}.

4.1.2.2 Small-Signal Analysis

We next linearize the phase difference θ_v about the steady state value $\theta_{v,s}$. We drop the subscript v in θ_v. The small-signal model for the VCO control system is shown in figure 4.5. SCL1 is locked to the master laser in OPLL1 and its phase noise ϕ_{s1} is given by equation (2.12):

$$\phi_{s1}(s) = (\phi_m(s) + \phi_{RF}(s))\frac{G_L(s)}{1+G_L(s)} + \phi_{s1}^{fr}(s)\frac{1}{1+G_L(s)}, \tag{4.12}$$

where we have substituted $G_L(s)$ for $G_{op}(s)$, and neglected ϕ_{e0}. The free-running phase noise of the VCO and the slave SCL2 are denoted by ϕ_{vn} and ϕ_{s2}^{fr} respectively.

[1] The loop locks stably only for $\theta_{v,s}$ on one side of zero.

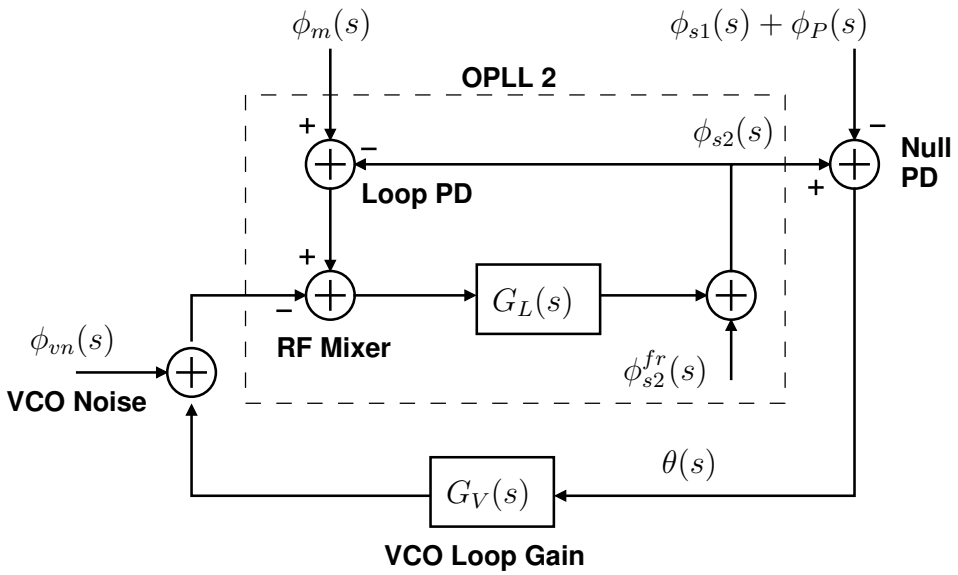

Figure 4.5. Small-signal phase model for the power-combining scheme with the additional VCO loop. SCL1 is locked to the master laser in OPLL1, and is not shown here. PD: Photodetector.

The variation in the differential path lengths traversed by the outputs of SCL1 and SCL2 produces a phase noise at the fiber combiner, and this noise has the Laplace transform $\phi_P(s)$. The OPLL open-loop gain is the same as G_L, and the gain $G_V(s)$ in the VCO branch is

$$G_V(s) = -\frac{K_v \sin\theta_{v,s} e^{-s\tau_v}}{s}, \tag{4.13}$$

where τ_v is the delay in the VCO branch (from the Null photodetector to the RF mixer) and $\theta_{v,s}$ is as in equation (4.10). Note that there is a trade-off in the choice of the value of $\theta_{v,s}$: a smaller $\theta_{v,s}$ results in a higher power combination efficiency, but also results in a lower loop gain. The reduction in loop gain can be compensated by increasing the DC gain K_v.[2]

The model in figure 4.5 can be solved for the variation in the output phase $\theta(s)$ to yield

$$\theta(s) = \frac{1}{1 + G_L + G_L G_V} \left(\begin{array}{l} \phi_{s2}^{fr} + G_L\left(\phi_m - \phi_{vn}\right) \\ \quad -\left(1 + G_L\right)\left(\phi_{s1} + \phi_P\right) \end{array} \right). \tag{4.14}$$

[2]The minus sign in equation (4.13) is present only for bookkeeping; in this case, the system locks with a negative $\theta_{v,s}$.

The argument s has been dropped from all the terms on the right-hand side. We substitute for $\phi_{s1}(s)$ using equation (4.12) to obtain

$$\theta(s) = \frac{1}{1 + G_L + G_L G_V} \left(\left(\phi_{s2}^{fr} - \phi_{s1}^{fr} \right) + G_L \left(\phi_{RF} - \phi_{vn} \right) - \left(1 + G_L \right) \phi_P \right). \quad (4.15)$$

To obtain some physical insight into the above equation, we note that the delay in the VCO loop τ_v is typically much larger than the OPLL delay. This limits the VCO open-loop gain G_V, so that the approximation $|G_L| \gg |G_V|$ holds at all frequencies. The denominator in equation (4.15) can then be expressed as $(1 + G_L)(1 + G_V)$, and we can rewrite the equation as

$$\theta(s) \approx \frac{1}{1 + G_L} \left(\phi_{s2}^{fr} - \phi_{s1}^{fr} \right) + \frac{1}{1 + G_V} \left(\phi_{RF} - \phi_{vn} - \phi_P \right). \quad (4.16)$$

Firstly, the master laser phase noise does not appear in the equation above. This is clear, since each slave SCL is locked to the master, and they beat with each other. Next, the phase noise of the free-running lasers is mainly suppressed by the OPLLs. Further, the VCO noise and phase noise introduced by differential path length delays are suppressed by the loop with transfer function $G_V(s)$. This is consistent with the interpretation that the system is the combination of three phase-locked loops: The slave lasers SCL1 and SCL2 are locked to the master laser using two heterodyne OPLLs at offsets given by ω_{RF} and ω_v respectively; and the VCO (along with other phase noise sources) is then locked to the RF offset frequency ω_{RF} in a third "outer" PLL. The laser phase noise is suppressed by the OPLLs, while the phase jitter of the VCO and the variation ϕ_P in the differential optical path length are suppressed by the third PLL.

4.1.3 Combining Efficiency

The power combination approach presented above can be scaled to a large number of lasers using a binary tree configuration as shown in figure 4.6. Fiber amplifiers can be used at the output of each slave SCL to increase the overall combined power. The

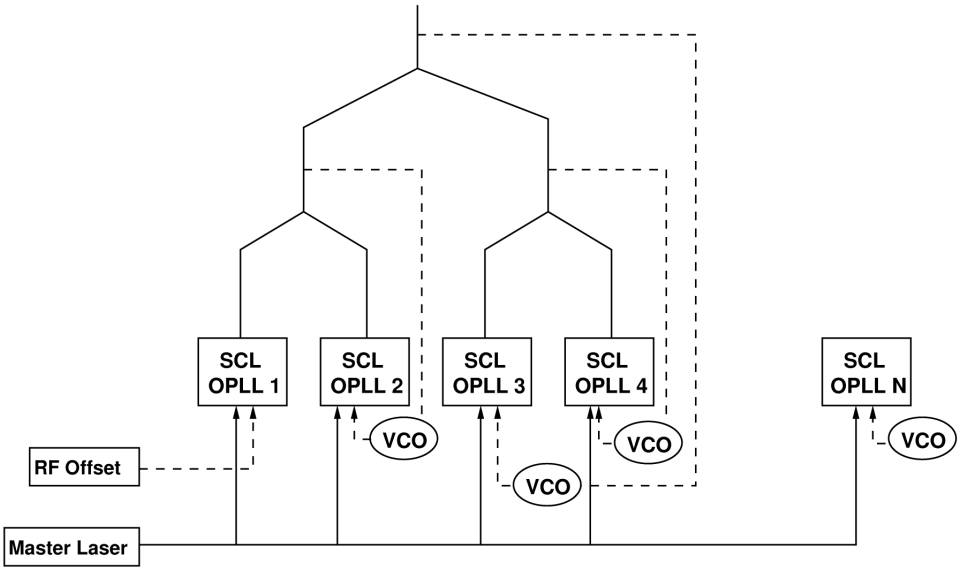

Figure 4.6. Binary tree configuration for the power combination of a number of SCLs locked to a common master laser in the filled-aperture configuration.

addition of fiber amplifiers increases the delay in the outer VCO loop, but the resultant bandwidth is still sufficient to correct for the slow fluctuations in the differential optical path length introduced by the amplifiers. We measured no additional phase noise when fiber amplifiers with output powers of ∼1 W were used at the outputs of the SCLs, and this is consistent with observations by other workers using narrow-linewidth seed lasers [104–106]. Our collaborators at Telaris have demonstrated the coherent combination of 4 fiber-amplified (35–40 W) semiconductor lasers using this approach to achieve a coherent and diffraction limited power output of ∼110 W.

The overall power-combining efficiency for two SCLs is affected by the intensity noise, relative polarizations and relative phase error between the combining beams, but is mainly limited by the phase noise of the combining beams. From equation (4.1), assuming that the deviations of the relative phase about the ideal value of zero are small, the efficiency of combining two optical beams is given by

$$\eta = \frac{P_c}{2P_0} \approx 1 - \frac{\langle \theta^2 \rangle}{4}. \tag{4.17}$$

The mean-squared value of the relative phase, $\langle \theta^2 \rangle$, has two important contributions:

(i) the steady state phase $\theta_{v,s}$ given by equation (4.10), and (ii) the residual phase noise of both the semiconductor lasers and the VCO, given by equation (4.15). The value of $\theta_{v,s}$ can be reduced by the use of cleaner VCOs and by the use of loop filters to increase the DC gain K_v. The residual phase noise of the SCLs can be reduced by increasing the OPLL loop bandwidth.

Let us briefly consider the effect of the residual phase error in the loop on the combination of a large number N of SCLs, e.g., as in figure 4.6. The output of slave SCL i is

$$E_i = \exp(j\omega_0 t + j\phi_0 + j\phi_{i,n}), \tag{4.18}$$

with ω_0 and ϕ_0 denoting the frequency and phase of the master laser (offset by the RF signal), and $\phi_{i,n}$ is the residual phase error in OPLL i. For simplicity, we have normalized the amplitude to unity. The total intensity is given by

$$I = \left\langle |E|^2 \right\rangle = \left\langle \left(\sum_{i \neq k}^{N} \exp(j\phi_{i,n} - j\phi_{k,n}) \right) \right\rangle + N. \tag{4.19}$$

For $i \neq k$, $\phi_{i,n}$ and $\phi_{k,n}$ are independent identically distributed random variables, assuming that the OPLLs are identical. Further, we have for a zero-mean Gaussian random variable X with variance σ^2, $\langle \exp(jX) \rangle = \exp(-\sigma^2/2)$. Therefore,

$$I = N + N(N-1)e^{-\sigma_\phi^2} \approx N^2 - N(N-1)\sigma_\phi^2. \tag{4.20}$$

The first term on the RHS is the combined power, and the second term denotes the reduction in efficiency due to residual phase error. The combining efficiency is therefore

$$\eta_c = 1 - \frac{N-1}{N}\sigma_\phi^2. \tag{4.21}$$

We conclude that the combining efficiency due to the residual phase noise in the OPLLs does not degrade with N, and reaches the asymptotic value $1 - \sigma_\phi^2$. Other sources of noise such as the frequency jitter of the VCOs and phase-front deformations caused by the optical elements used for beam-combining are analyzed in detail in

reference [66], and it is shown that minimizing these errors is critical to achieve large combining efficiencies.

4.1.4 Summary

We have presented an all-electronic active feedback approach for the coherent power combination of SCLs using OPLLs. Elements of an array of SCLs locked to a common master laser have the same frequency and phase and can be coherently combined. The phase of the combining SCLs is further controlled using an electronic VCO to compensate for differential path length variations of the combining beams. We have demonstrated the coherent combination of various high power SCLs using this approach, and have achieved a stable power-combining efficiency of 94%. The electronic feedback scheme demonstrated eliminates the need for optical phase or frequency shifters. It is possible to obtain coherent and diffraction limited power of tens of kilowatts by the use of fiber amplifiers to amplify the outputs of an array of phase-locked SCLs. When scaled to a large number of SCLs, the overall power combination efficiency is likely to be limited by VCO jitter and phase front deformations.

4.2 Optical Phased Arrays

Phased array antennas have had significant success in the RF domain for beam-forming, steering, communication and three-dimensional imaging applications. Analogous efforts and advances in the optical domain however, have had limited success. Past demonstrations of phased array beam-steering have required injection locking of the individual lasers elements in the array [107], which is inherently unstable and difficult to scale due to complexity and cost. An alternative method utilizing a single laser, which is expanded and passed through an array of phase modulators, results in limited output power [108]. Furthermore, the state-of-the-art for this method utilizes liquid crystal spatial light modulators, which have limited bandwidths.

The CBC approach developed in this chapter provides an alternative technology for optical phased arrays and beam-steering that has the potential to overcome the

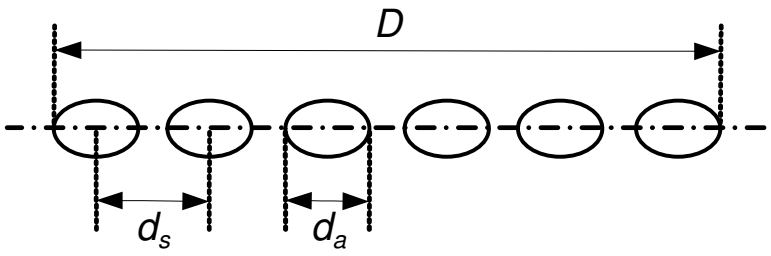

Figure 4.7. A one-dimensional array of coherent optical emitters.

fundamental challenges encountered by previous approaches. An array of SCLs is locked to a common master laser using heterodyne OPLLs, and the individual SCL outputs are placed side by side to form a larger aperture. Electronic phase shifters are utilized to control the phase of the offset signal to each OPLL, hence controlling the phase of each individual laser emitter and enabling electronic control over the optical wavefront. One can foresee a number of potential applications of this approach, including adaptive optics, control over the focusing distance, and fast and robust beam-steering for imaging and free-space data transfer.

4.2.1 Far-Field Distribution

We will limit ourselves to the discussion of a one-dimensional optical phased array, as shown in figure 4.7. A number, N, of coherent optical emitters are arranged along a straight line, with interemitter spacing d_s. The width of each aperture is d_a, and the total width of the optical aperture is D. We are interested in the far-field distribution of the optical intensity, along the axial direction. The far-field angular distribution of the field is simply a Fourier transform of the shape (and phase) of the aperture [109], and can be precisely calculated for the aperture shown in figure 4.7 [68]. Here, we only describe the salient features of the far-field distribution:[3]

- The far-field distribution consists of several lobes or fringes, each of which has an angular width $\theta_{lobe} \sim \lambda/D$, where λ is the wavelength of light. The finite size of the aperture creates "sublobes" around each lobe, and these sublobes

[3]This discussion assumes that $d_s \gg \lambda$. If this is untrue, the inherent approximation that $\tan\theta \approx \theta$, where θ is the angle in the far field, is no longer valid.

can be made smaller by apodizing the aperture.

- The size of each emitter, d_a, defines an overall angular envelope of width $\theta_{steer} \sim \lambda/d_a$, within which the beam may be steered.

- The lobes in the intensity distribution repeat with an angular pitch $\theta_{pitch} = \lambda/d_s$. Since d_s is always larger than d_a, there is always more than one lobe in the far-field distribution pattern. However, by making the ratio d_a/d_s, known as the "fill-factor," close to unity, the optical power can be consolidated into just one central lobe.

- If a linear phase ramp is applied to the aperture, i.e., if the phase of each emitter is offset from its neighbor by $\Delta\phi$, the position of the main-lobe in the far-field (the "beam") is given by $\theta_{beam} = (\Delta\phi/2\pi)(\lambda/d_s)$. This is the basis of beam-steering using an optical phased array. The beam can be steered by a maximum angle of λ/d_s, and an important figure of merit is the number of beamwidths by which the beam can be steered, given by D/d_s.

We use phase-locked SCLs as the coherent emitters in figure 4.7, and the phase of the laser is controlled by changing the phase of the offset signal in the heterodyne OPLL. The maximum speed of tuning is determined by the settling time of the loop, described in equation (2.19).

4.2.2 Experimental Results

The experimental setup for the demonstration of electronic beam-steering using OPLLs is shown in figure 4.8. Two slave DFB SCLs at 1539 nm (JDS-Uniphase, see table 2.1) are phase-locked to a common master laser (NP Photonics) at an offset frequency of 1.7 GHz. An RF phase shifter, used in one of the OPLLs, produces a phase shift of up to π radians. The outputs of the two phase-locked lasers are brought next to each other using a custom 8-channel single-mode fiber array (Oz Optics, Ottawa, Canada) with a channel spacing of 250 µm. The distance between the emitters, d_s, can be varied by choosing different channels of the fiber array. The output of the fiber array

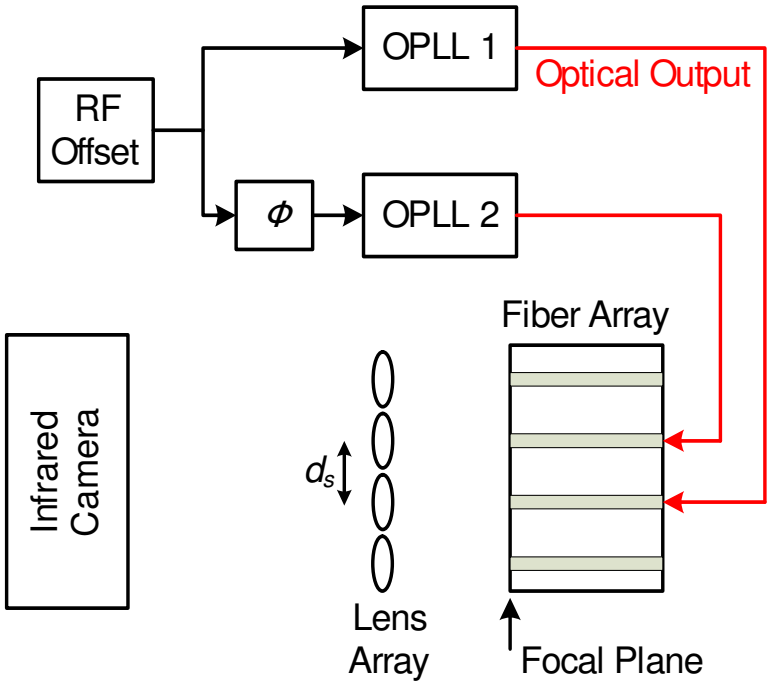

Figure 4.8. Experimental setup for the demonstration of beam-steering using OPLLs. The slave SCLs in the OPLLs are phase-locked to a common master laser. The phase of the RF offset signal into OPLL2 is controlled using an electronic phase shifter.

assembly is placed at the focal plane of a microlens array of the same pitch (Leister Technologies, Itasca, IL), and the resultant far-field distribution is measured using an infrared camera.

The measured intensities on the camera for the incoherent and coherent addition of the beams is shown in figure 4.9, for $d_s = 0.25$ mm.[4] The corresponding horizontal intensity distributions are shown in figure 4.10(a), where two important features should be noted. The coherently added far-field distributions show a peak intensity that is about twice the peak intensity of the incoherent case, and the size of the main lobe is reduced by a factor of two, as expected. Second, a change in the RF phase by π radians causes a steering of the beam by one-half the fringe separation, demonstrating that the change electronic phase results in a change in the optical phase in a one-to-one manner. Similarly, the horizontal intensity distribution for an emitter separation of $d_s = 0.5$ mm is shown in figure 4.10(b), showing that the fringe sepa-

[4]The images in figure 4.9 are not calibrated for the camera's nonlinear response. The calibrated traces are shown in figure 4.10.

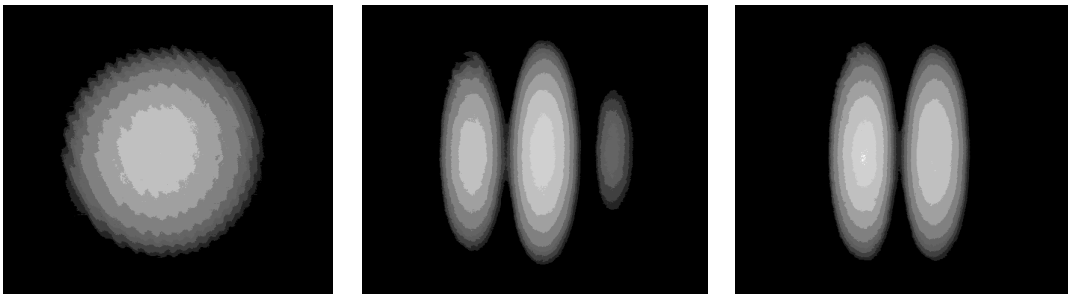

(a) (b) (c)

Figure 4.9. Measured far-field intensities on the infrared camera for $d_s = 0.25$ mm, when (a) one of the OPLLs is unlocked and (b), (c) both OPLLs are locked. The RF phase is varied between (b) and (c), demonstrating electronic steering of the optical beam.

ration reduces by a factor of two within the same envelope of the distribution. The nonideal fringe visibility (the minima do not go down to zero) is mainly a result of poor camera dynamic range, but other factors such as mismatched optical intensities, polarization states and residual phase errors in the OPLLs significantly reduce the visibility.

Modeling the laser outputs as Gaussian beams, the far-field intensity distribution is theoretically calculated [68] and compared to the experimental result in figure 4.11, showing excellent agreement. By choosing different channels of the fiber array, the far-field distributions are measured for different values of the emitter separation d_s. The variation of the experimentally measured fringe separation is plotted against the inverse emitter separation d_s^{-1} in figure 4.12, and the linear dependence is verified.

4.2.3 Effect of Residual Phase Noise on Fringe Visibility

Finally, we consider the effect of the OPLL residual phase noise on optical sidebands in the far field. Consider an optical phased array composed of N individual emitters, labeled $1, 2, \ldots, N$, where each emitter is a SCL phase-locked to the master laser in an OPLL with residual phase error σ_ϕ^2. The effect of a varying steady-state phase error can also be included in this variance. At a point $\vec{r}$ in the far field of the phased

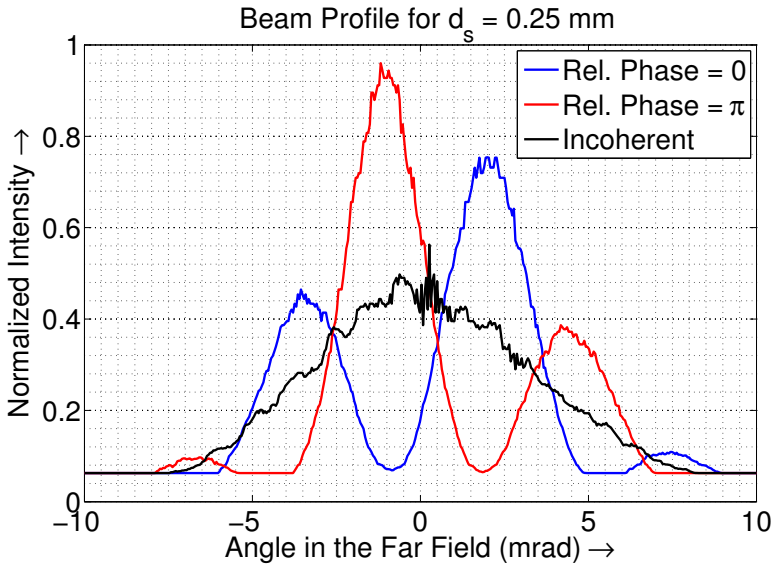

(a)

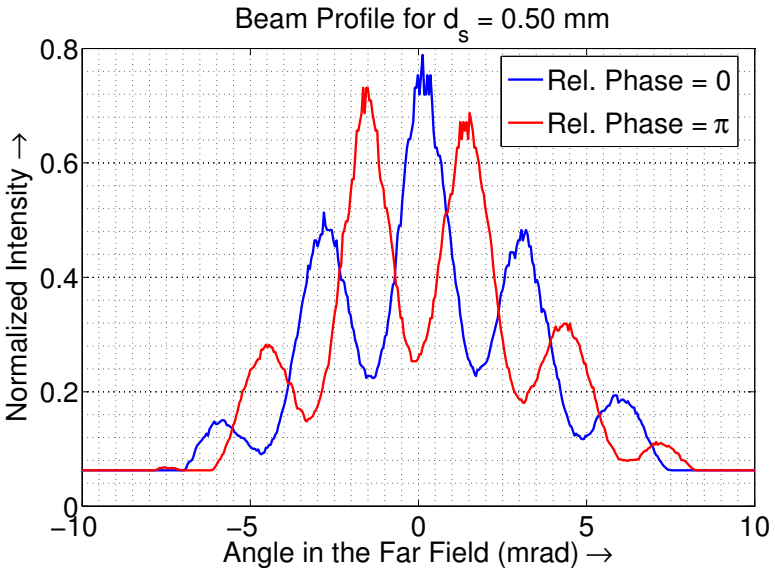

(b)

Figure 4.10. Horizontal far-field intensity distributions demonstrating beam-steering of half a fringe by an RF phase shift of π radians, for emitter spacings of (a) $d_s = 0.25$ mm and (b) $d_s = 0.5$ mm. The incoherently added intensity distribution is also shown in (a).

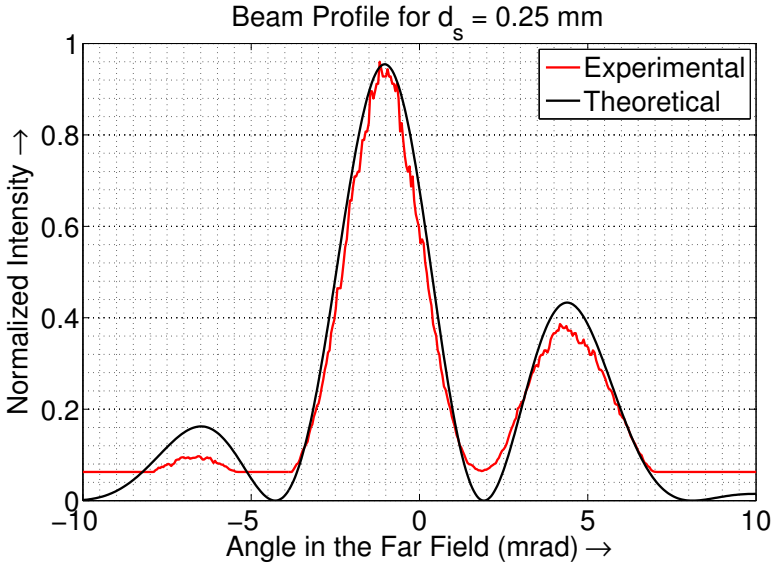

Figure 4.11. Comparison of the experimental far-field intensity distribution with the theoretical calculation.

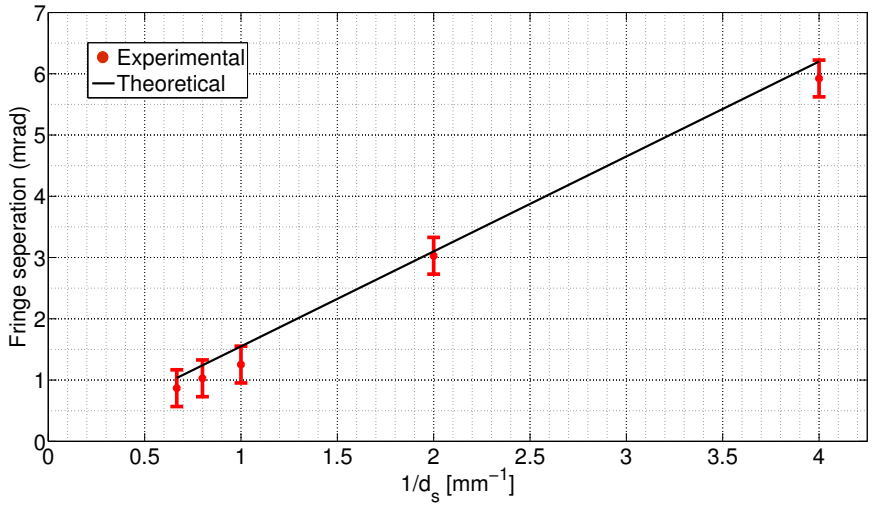

Figure 4.12. Separation between fringes as a function of the inverse beam separation d_s^{-1}, compared to theory.

array aperture, let the field due to emitter i be given by

$$E_i = a_i \exp(j\omega_0 t + j\phi_i + j\phi_{i,n}), \tag{4.22}$$

where a_i and ω_0 denote the amplitude and frequency of emitter i, ϕ_i is the phase of the wave *at the point* $\vec{r}$ (controlled by RF phase shifters), and $\phi_{i,n}$ denotes the phase noise due to emitter i, which is not corrected by the OPLL. $\phi_{i,n}$ is a zero-mean Gaussian random variable with standard deviation σ_ϕ^2. For simplicity, we will assume that the amplitudes a_i are equal to unity; a more general result can easily be derived. The total field at the point $\vec{r}$ is given by $E = \sum_{i=1}^{N} E_i$, and the time averaged intensity is given by

$$I = \left\langle |E|^2 \right\rangle = \left\langle \left(\sum_{i=1}^{N} \exp(j\phi_i + j\phi_{i,n}) \right) \left(\sum_{k=1}^{N} \exp(-j\phi_k - j\phi_{k,n}) \right) \right\rangle. \tag{4.23}$$

The phases ϕ_i are constant over the averaging interval, so that

$$I = \sum_{i \neq k}^{N} \left[\exp(j(\phi_i - \phi_k)) \left\langle \exp(j(\phi_{i,n} - \phi_{k,n})) \right\rangle \right] + N. \tag{4.24}$$

For $i \neq k$, $\phi_{i,n}$ and $\phi_{k,n}$ are independent random variables. Further, we have for a zero-mean Gaussian random variable X with variance σ^2, $\langle \exp(jX) \rangle = \exp(-\sigma^2/2)$. Therefore,

$$I = N + e^{-\sigma_\phi^2} \sum_{i \neq k}^{N} \exp(j(\phi_i - \phi_k)). \tag{4.25}$$

The intensity pattern in the far field consists of maxima and minima according to how the phases in equation (4.25) add up. Let us first assume no phase noise, i.e., $\sigma_\phi = 0$. At a maximum, all the phases add in phase ($\phi_i = \phi_k$) to give

$$I_{max} = N + N(N-1) = N^2. \tag{4.26}$$

At a minimum, we have zero intensity, so that

$$I_{min} = 0 = N + \sum_{i \neq k}^{N} \exp(j(\phi_i - \phi_k)). \tag{4.27}$$

We now consider phase noise. With the addition of phase noise, the intensity at a maximum is

$$\begin{aligned} I_{max,n} &= N + N(N-1)e^{-\sigma_\phi^2} \simeq N + N(N-1)(1-\sigma_\phi^2) \\ &= N^2 - (N^2 - N)\sigma_\phi^2, \end{aligned} \tag{4.28}$$

which is also the result for the CBC efficiency in equation (4.21). At a minimum,

$$\begin{aligned} I_{min,n} &\simeq N + (1-\sigma_\phi^2) \sum_{i \neq k}^{N} \exp(j(\phi_i - \phi_k)) \\ &= N + (1-\sigma_\phi^2)(-N) = N\sigma_\phi^2. \end{aligned} \tag{4.29}$$

We have used equation (4.27) in deriving the above. The ratio of the maximum to the minimum intensity is therefore

$$\frac{I_{max,n}}{I_{min,n}} = \frac{N - (N-1)\sigma_\phi^2}{\sigma_\phi^2}. \tag{4.30}$$

Note that we have made no assumptions about the location of the N emitters in the array. We have only assumed that the interference pattern in the absence of noise produces nulls, an assumption which is valid when the emitters have equal (or symmetric) amplitudes. The ratio derived above sets an upper bound on the maximum achievable sideband suppression ratio. In an aperture with emitters of equal power, the finite size of the aperture creates sidebands. With an apodized aperture, the strength of these sidebands can be reduced until the above limit is reached.

The practical realization of optical phased arrays requires a large number of elements (from tens to hundreds in one dimension), and is a major technological chal-

lenge. It will require the fabrication of arrays of narrow-linewidth SCLs. For example, there has been some progress in the fabrication of large-scale independently addressable vertical cavity surface-emitting laser (VCSEL) arrays [110, 111]. Integrated OPLLs have recently been demonstrated by various workers [22, 23, 77]. We believe that it is feasible to use integrated optical waveguides to combine the outputs of many discrete phase-locked SCLs residing on a single chip to form a single coherent aperture with narrow spacing between adjacent emitters and electronic control over the phase of each emitter in the aperture.